SLOPE STABILITY 2024
BELO HORIZONTE - BRASIL

April 14 to 19, 2024

Fundação Dom Cabral
Nova Lima, Minas Gerais, Brazil

Synthetic rock mass modeling of progressive unravelling and overall slope stability using the discrete element method

Rami Abousleiman *Knight Piésold and Co., Denver, USA*

Carlos Contreras *Stantec, Lima, Peru*

Jim Cremeens *Knight Piésold and Co., Denver, USA*

Abstract

Mining of epithermal gold deposits often encounters a wide range of rock mass conditions in a single excavation. Selecting the appropriate representation for design and analysis in variable ground conditions is critical. Continuum representation of rock masses in numerical or analytical methods used in state-of-practice slope design simplify the complex relationship between intact rock and discontinuities. Continuum methods are generally accepted for end-member strong or weak rock masses but cannot explicitly consider the effect of discontinuity orientation, separation, and material bulking on slope stability. Discontinuum methods often require the user to provide pre-determined failure surfaces, which can bias the model results when used for predictive modeling or design. Hybrid methods exist, but can require significant computational power and require extensive calibration.

This study utilizes the synthetic rock mass (SRM) approach by combining the Generalized Hoek-Brown and Mohr-Coulomb Strain Softening constitutive models available in Itasca's Universal Distinct Element Code (UDEC) to represent intact material and discontinuities, respectively. Where appropriate, discontinuities were assigned an equivalent Mohr-Coulomb strength based on previously developed Hoek-Brown parameters during initial domain development for pit slope angle recommendations. The numerical model was used to analyze a case study from an open-pit gold mine failure of a weak, in-dipping fault-zone that resulted in the propagation of failure and unravelling of a 18 m bench of otherwise competent rock. Numerical model results were compared to the observed deformation and survey monument displacement data. Following confirmation of realistic model behavior, the model was used to evaluate the design of a proposed layback and buttress to continue mining safely.

1 Introduction

Knight Piésold and Co. (Knight Piésold) provides rock mechanics engineering support to an active gold mine referred to herein as Mine A. Mine A's main pit is hosted in high sulfidation epithermal ore deposits. During the first quarter (Q1) 2022, multiple low-flow seeps and damp bench faces associated with single bench failures were observed along multiple benches at the west wall of the main pit. Failures were related to perched groundwater in two low-strength fault zones (FZ).

A revised geotechnical and hydrogeological model was developed through additional site investigations and the impact of groundwater on overall slope stability was assessed via Limit Equilibrium models (Spencer 1967, RocScience 2022). The results of the pit slope stability evaluation indicated that the previous recommendations for pit slope angles remained valid with the addition of groundwater to the model, but that bench scale failures were likely to continue where perched water and fault zones intersected. Knight Piésold noted that propagating or unraveling failure was possible in dry areas outside of fault zones if competent benches were undermined.

During the second quarter (Q2) 2022, multiple localized bench-scale failures within the west wall fault zones, FZ1 and FZ2, were reported. Unraveling propagated to the double bench in competent rock (Upper Tuff) immediately above FZ1 (Figure 1).

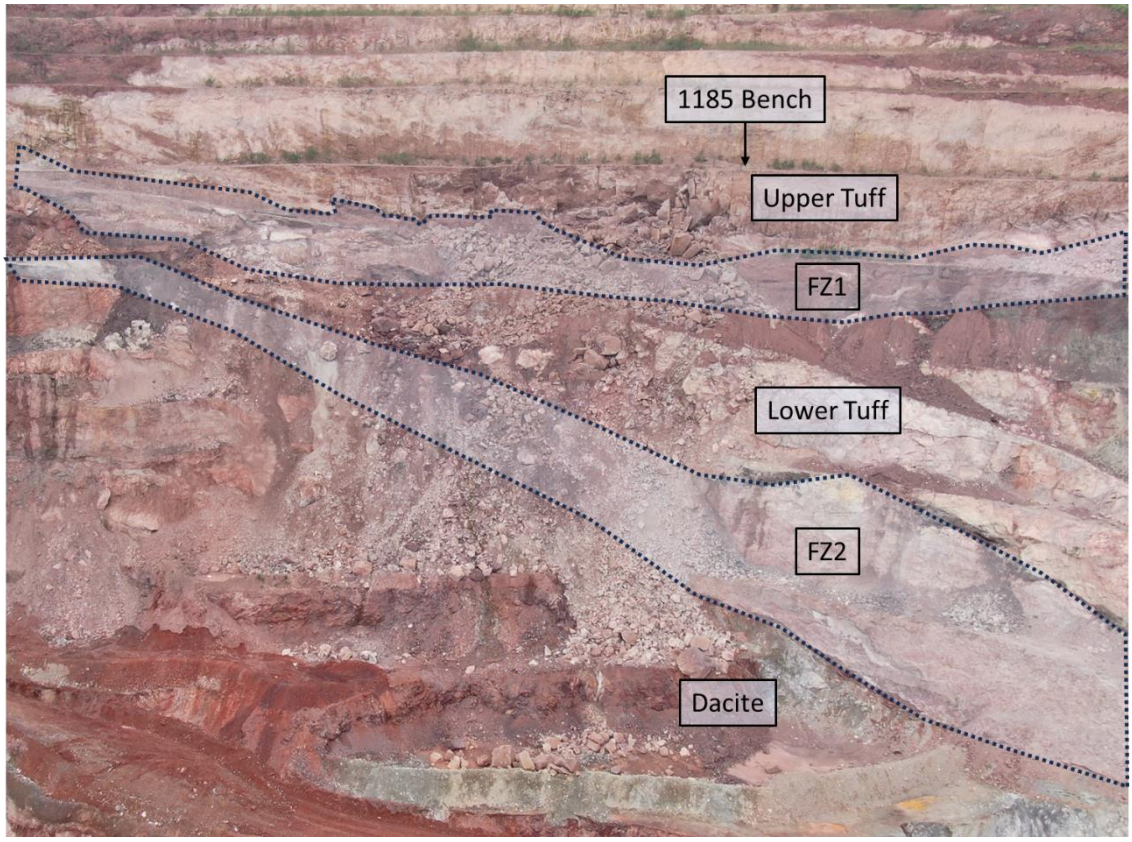

Figure 1. Post-failure image annotated with relevant geologic units, fault zones, and bench elevations.

Mine A proposed a layback of the slope to remove rockfall sources and construction of a buttress to prevent continued failure initiation within FZ1 and FZ2. Knight Piésold analyzed the stability of the proposed construction using a discrete element method (DEM) numerical model based on the geotechnical data available from previous site investigations and slope stability evaluations, site-specific observations collected by Knight Piésold personnel during multiple site visits, as well as geologic and prism monitoring (slope displacement) information provided by Mine A.

The synthetic rock mass (SRM) approach was implemented with the DEM to explicitly capture both the observed unravelling of competent benches above the fault zones, and the measured displacement above the slope above the failing benches. Following limited model calibration and confirmation of representative model behavior, the shear strength reduction method was implemented to evaluate the factor of safety of the proposed layback and buttress under static and pseudo-static loading conditions.

2 Geologic Setting

The Mine A open pit trends along a north-south oriented ridge and exploits a hydrothermal ore deposit hosted in pyroclastic, volcaniclastic, and volcanic rocks. Lithologies exposed by excavation of the west wall include basalt, lithic tuff, and vitric tuff, which is underlain by a suite of altered tuffs, breccias, and rhyodacite porphyry. The alteration sequence includes silicic, vuggy silicic, advanced argillic (pyrophyllite and dickite), argillic (kaolinite and illite), and propylitic assemblages.

Major fault zones influence the rock mass strength and groundwater flow in the west wall. There are two fault zones that dip into the west wall, FZ1 and FZ2. FZ1 traverses the central and southern portions of the west wall, striking northwest and dipping approximately 40 degrees to the west. FZ2 strikes sub-parallel to FZ1 and dips to the west at approximately 70 to 80 degrees. FZ1 and FZ2 are directly related to the instability assessed in this study.

3 Methodology

The observed failure mechanisms in the slope relied on a combination of moment-driven deformation (Cremeens 2003) along weak rock mass and structure (i.e., FZ1 and FZ2), exacerbated by perched groundwater, ultimately resulting in failure of fault zones propagating to discontinuity-driven unravelling of more competent rock mass. To capture the relevant mechanisms, Knight Piésold selected the two-dimensional DEM software UDEC (Itasca 2019) to represent the rock mass as an assemblage of discrete blocks. The block contacts were assigned independent material properties to capture the effect of a variety explicit discontinuities on the deformation of the rock masses. Block contacts in the model presented herein were related to the strength of the intact material to allow for realistic propagation of rock mass yield and failure through the model according to the SRM approach.

1.1 Model Geometry and Cases

The stability assessment included the following analyses: (1) static back analyses, which involved capturing the observed mechanisms and extent of slope deformation; and (2) static and pseudo-static analyses after the proposed stabilization, which evaluated the effectiveness of the buttress construction and unloading of the upper sector of the slope to stabilize the failed sector.

Numerical models in UDEC were developed for a cross-section of the west wall, selected to represent the critical configuration of the unstable area. The models' geometry and stratigraphy correspond to the topographic and geological information provided by Mine A (Figure 2).

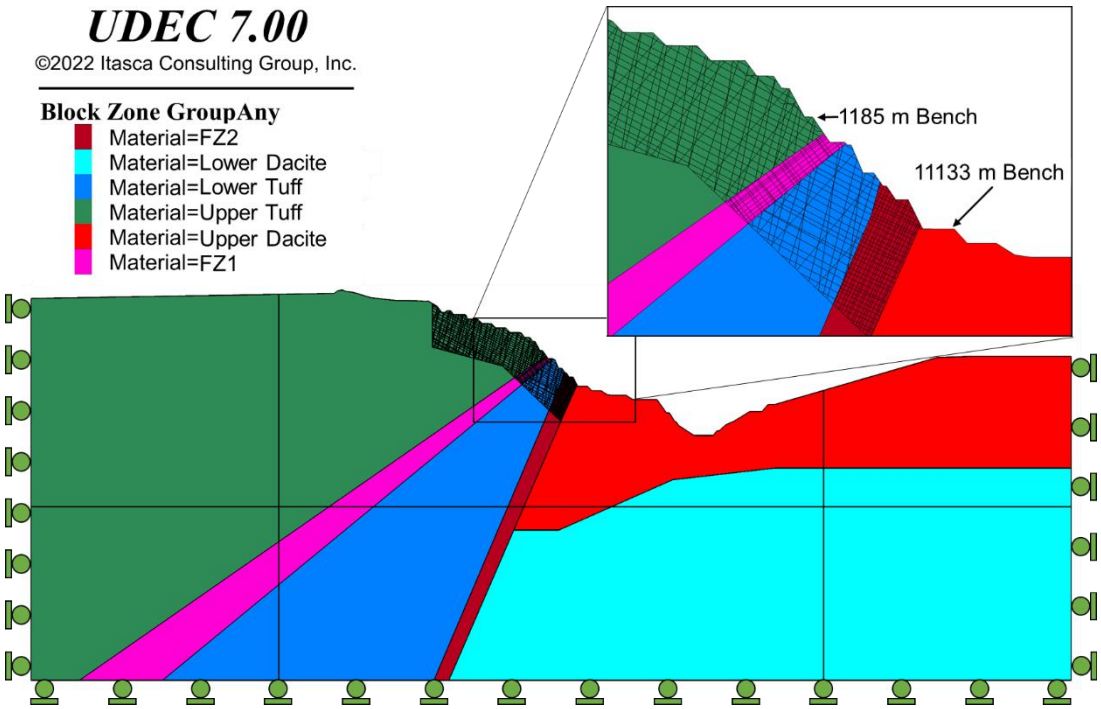

Figure 2. Pre-failure model geometry depicting model lithologies and boundary conditions, detail view showing where explicit discontinuities were modeled.

Although the initial modeled failures in FZ1 and FZ2 were coincident with perched groundwater, propagation of failure and unravelling of the benches above the fault zones was not coincident with observed seeps. Numerical models were developed under completely dry (drained) conditions, which did not allow for failure to propagate from FZ2 through the Lower Tuff, to FZ1. To account for this lack of failure in the static back analysis, the contact shear strength properties of the FZ1, FZ2, and Lower Tuff lithologies in the slope were decreased until localized failure (in tension and/or shear) of the modeled contacts (discontinuities) led to a larger deformation of the slope between the 1185 and 1113 m benches, mimicking the behavior seen in the field.

Slope prism displacement data were used to adjust the resulting displacement orientations within the 1185 and 1231 m benches and confirm that the back-analysis model was capturing the observed behavior.

The models for these analyses represent the geometry of the slope after unloading the upper sector of the slope (i.e., mining the slope between the 1221 and 1185 m benches) and placing a buttress at the toe of the failed sector (Figure 3), while the contacts within the failed zone were modeled in a residual shear strength state.

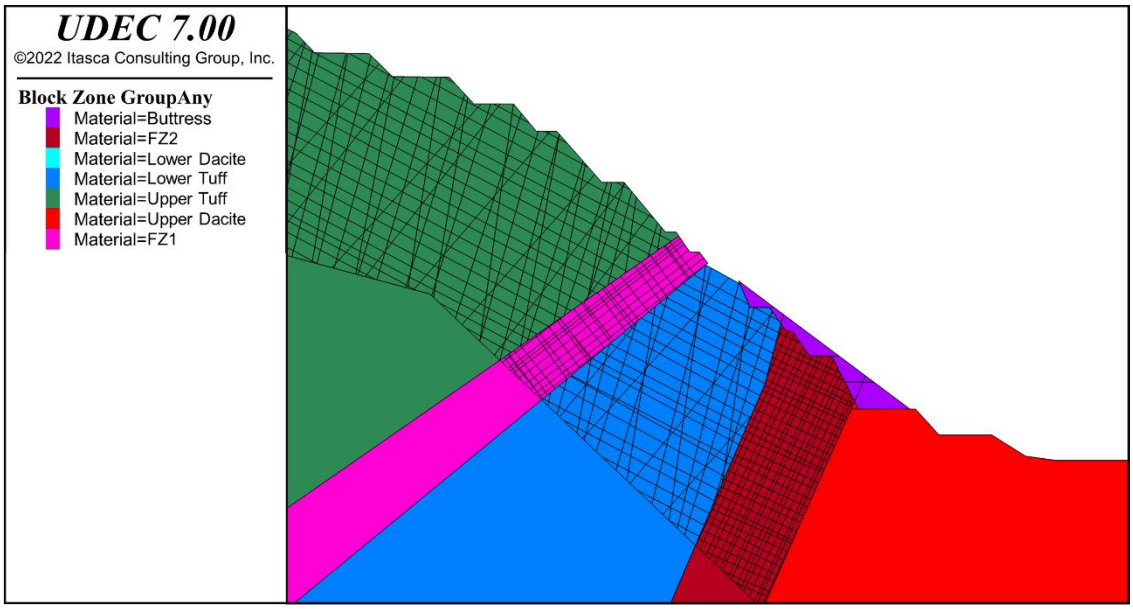

Figure 3. Detail view of post-failure geometry model, with layback excavated and buttress installed.

The shear strength reduction (SSR) method implemented in UDEC was employed to define the factor of safety (FOS) of the model geometry depicted in Figure 3. UDEC applies the SSR method under a bracketing approach to determine the boundary between physical stability and instability, through a set of simulations run with different strength-reduction factors (Itasca 2019).

1.2 Model Inputs

UDEC models require defining block and contact strength and stiffness properties. Knight Piésold used the properties defined for the slope stability evaluation for the west wall during previous design stages as a basis for the development of properties for the UDEC models assessing the buttress and layback stability.

1.2.1 Rock Mass Block Properties

Material properties were developed based on geotechnical and hydrogeological field and laboratory data collected during previous site investigations.

A shear strength vs. normal stress relationship for rock mass was developed for each engineering lithology using the Generalized Hoek-Brown failure criterion (Hoek et al. 2002). This relationship is defined using a combination of uniaxial confined strength (UCS) and Primary Hoek-Brown parameters. The UCS and the Primary Hoek-Brown parameters were incorporated into the geotechnical model used for limit equilibrium stability analyses. Primary Hoek-Brown input parameters include Geological Strength Index (GSI), a material strength constant (m_i), and a disturbance factor (D) as defined by Marinos and Hoek (2000). Secondary Hoek-Brown parameters (a, s, m_b) were calculated as follows. The disturbance factor, D was assumed to be zero and tensile strength was defined assuming a value of 0.1 times the equivalent cohesion for a maximum confining stress at a depth of 100 m.

Stiffness properties such as Young's modulus (E) and Poisson's ratio (v) were defined based on empirical estimations (Hoek and Diederichs 2006) and average values of similar materials (Kulhawy 1975), respectively. Shear modulus (G) and bulk modulus (K) were estimated from E. Table 1 summarizes the properties applied to the rock mass blocks.

Table 1. Hoek-Brown material properties applied to intact rock mass blocks.

Parameter	Material			
	Tuff	Upper Dacite	Lower Dacite	Basalt
Density, ρ (kg/m3)	2620	2620	2620	2426
Poisson's Ratio, v	0.2	0.2	0.2	0.2
Young's Modulus, E (GPa)	6.9	4.1	7.4	8.9
Bulk Modulus, K (GPa)	3.9	2.3	4.1	5.0
Shear Modulus, G (GPa)	2.9	1.7	3.1	3.7
Uniaxial Compressive Strength, UCS (MPa)	50.1	16.2	30.3	49.3
Geological Strength Index, GSI	52.0	65.0	64.0	57.0
Material Constant m_i	21.0	25.0	25.0	25.0
Disturbance Factor, D	0.0	0.0	0.0	0.0
Material Constant a	0.505	0.502	0.502	0.504
Material Constant s	0.0048	0.0205	0.0183	0.0084
Material Constant m_b	3.78	7.16	6.91	5.38
Dilation Angle to Friction Angle Ratio, ψ/ϕ	0.125	0.125	0.125	0.125

Itasca's Plastic Shear Strain, e^{ps} (mstrain)	30	30	30	30
Tensile Strength, σt (MPa)	0.1	0.08	0.11	0.11

1.2.2 Fault Zone Block Properties

A shear strength vs. normal stress relationship for residual rock was developed for the FZ2 and FZ1 using the Mohr-Coulomb failure criterion. The relationship between shear strength and effective normal stress is defined by the effective cohesion and effective friction angle. The effective friction angles were estimated from laboratory testing. Laboratory testing included particle size distribution and isotropically consolidated undrained triaxial (TX-ICU) testing of disturbed fault zone material. Testing was conducted per ASTM guidelines by Knight Piésold's geotechnical laboratory in Denver, Colorado. TX-ICU were conducted at effective confining stresses of approximately 100, 500, and 1,000 kilopascals (kPa). This range of confining stresses was selected to span estimated ranges of in-situ stresses that will be developed within the fault zones and to reasonably define the characteristics of the fault material shear strength envelopes.

Shear strength properties were calculated using the Mohr-Coulomb criterion and assuming zero apparent cohesion. Coarse-grained and fine-grained FZ2 material had peak effective friction angles of 29.7 degrees and 22.3 degrees, respectively. These peak effective friction angles were selected based on the most conservative best fit interpretation of a linear failure envelope to the peak obliquity (ratio of major to minor effective principal stress) measured during shearing. For the numerical models, FZ2 and FZ1 blocks were modeled with the Mohr-Coulomb constitutive model. A friction angle (Φ) of 30 degrees and cohesion (c) of zero were used. Stiffness properties were defined based on experience with similar materials and engineering judgment. Table 2 summarizes the properties applied to the FZ2 and FZ1 blocks.

Table 2. Mohr-Coulomb material properties applied to fault zone blocks and buttress material.

Parameter	**Material**	
	Fault Zones	**Buttress**
Density, ρ (kg/m3)	1600	2100
Poisson's Ratio, v	0.34	0.35
Young's Modulus, E (GPa)	0.9	0.9
Bulk Modulus, K (GPa)	1.0	1.0
Shear Modulus, G (GPa)	0.3	0.3
Friction Angle, φ (°)	30	38
Cohesion, c (MPa)	0	0
Tensile Strength, σ_t (MPa)	0	0

1.2.3 Discrete Fracture Network Properties

Discrete fracture networks (DFN) were implemented to allow for realistic separation of the rock mass and fault zone material following yield and failure. Rock mass DFNs were based on joint sets and spacing identified in two oriented core drillholes. Four joint sets were identified including one joint set dipping towards the pit at a low angle and three joint sets dipping towards the slope at a high angle. The high dip angle joint set corresponds to the high dip angle of the adjacent FZ2.

The DFNs implemented in the Fault Zones were significantly simplified to allow for sliding perpendicular to the dip of FZ1 and FZ2. Joint set orientation and spacing were defined based on experience with similar materials and engineering judgment because oriented core data within the fault zones was not available. One joint set that is sub-parallel to the fault dip and a second joint set that is sub-orthogonal to the first set were used. Table 3 summarizes joint set orientations and spacings used for DFN generation. Note that joints were modelled as fully persistent with no assigned gap and standard deviations were adjusted to prevent bad geometry blocks from forming during stochastic generation.

Table 3. Summary of joint set dip and spacing for DFN generation.

Material	Joint Set ID	Dip (°)		Spacing (m)	
		Mean	Standard Deviation	Mean	Standard Deviation
Tuff	Set 1	28	1	4	1
	Set 2	80	2	14	5
	Set 3	74	2	8	3
	Set 4	50	3	17	6
FZ2	Set 1	37	-	2	1
	Set 2	53	2	3	1
FZ1	Set 1	65	-	2	1
	Set 2	25	2	3	1

1.2.4 Discontinuities

All contacts representing DFN joints and contacts between the different lithologies were modeled with the Mohr-Coulomb constitutive model. The FZ2 and FZ1 contacts (Φ = 30° and c = 0) were adopted from the values used for the FZ2 and FZ1 blocks. The normal stiffness (kn) and shear stiffness (ks) of contacts were defined using the method suggested by Itasca (2019) based on the stiffness of contiguous blocks.

For the joints in Tuff, Mohr-Coulomb shear strength properties (Φ and c) were estimated from the block Hoek-Brown parameters. The equivalent Mohr-Coulomb properties were developed using the procedure proposed by Hoek et al. (2002), which consists in fitting a linear Mohr-Coulomb envelope to the non-linear Hoek-Brown failure envelope for a specific stress range. The calculations involve defining a maximum confining stress ($\sigma 3_{max}$) or upper limit for the stress range

proportional to the slope height. The relationship between the Mohr-Coulomb and Hoek-Brown varies in proportion to the $\sigma 3_{max}$ value and should be calculated for each specific case.

The Upper Tuff (above the FZ1) was assumed minimally disturbed based on the use of pre-splits for design bench blasting with strength minimally affected. Equivalent Φ and c for the contacts in this sector were estimated using a D of 0 and $\sigma 3_{max}$ for a slope height of 100m (Hoek et al., 2002). The tensile strength was assumed equal to 0.1 times c, which is a typical and reasonable value. The Lower Tuff (i.e., between FZ1 and FZ2) was assumed to present significant degree of disturbance between the two fault zones and the strength of the contacts in this unit was assumed to be frictional based on observed failure in the field. The contact properties applied in the models are summarized in Table 4.

Table 4. Stiffness and Mohr-Coulomb shear strength properties applied to discontinuity contacts.

Parameter	Material			
	Upper Tuff	Lower Tuff	Fault Zones	Buttress Contacts
Normal Stiffness, kn (GPa/m)	2.6	2.6	0.5	1.1
Shear Stiffness, ks (GPa/m)	1.1	1.1	0.2	0.4
Peak Friction Angle, φ_p (°)	52	38	30	38
Peak Cohesion, c_p (MPa)	1.0	0.0	0.0	0.0
Peak Tensile Strength, σ_{tp} (MPa)	0.1	0.0	0.0	0.0

The strength parameters of contacts or discontinuities represented in the models were adjusted to recreate the failure mechanism observed in the site visits and drone photographs. The strength parameters applied to these discontinuities were varied until a group of blocks failed along their contacts within the limits observed in the field at the 1185 and 1113 m benches and the displacements recorded on survey prisms above the failed areas were in agreement with modeled results.

4 Results

Results of the pre-stabilization models show that the models are dominated by tensile failures along the sub-vertical discontinuities within the Lower Tuff, FZ1, and FZ2, which indicate moment-driven deformations. Figure 4 shows the joint failure state dominated by tensile strength in the sub-vertical joints.

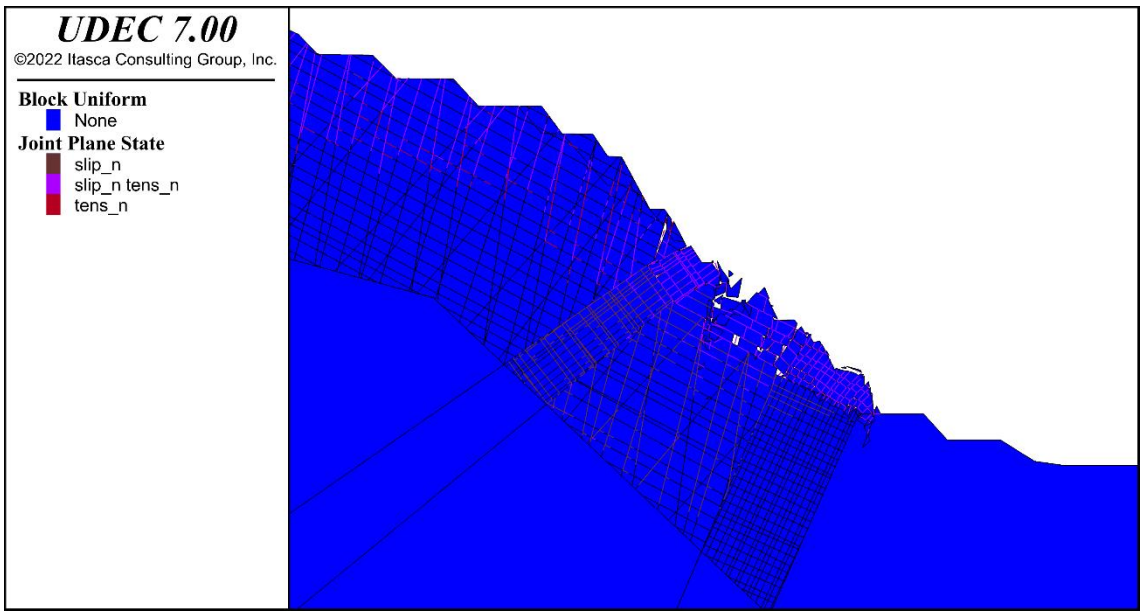

Figure 4. Model joint plane state during failure.

The model representing the highly disturbed rock mass in the lower tuff case resulted in a relatively deep failure boundary, Figure 5 presents the displacement contours, movement direction vectors, and block detachment that limits the failure masses.

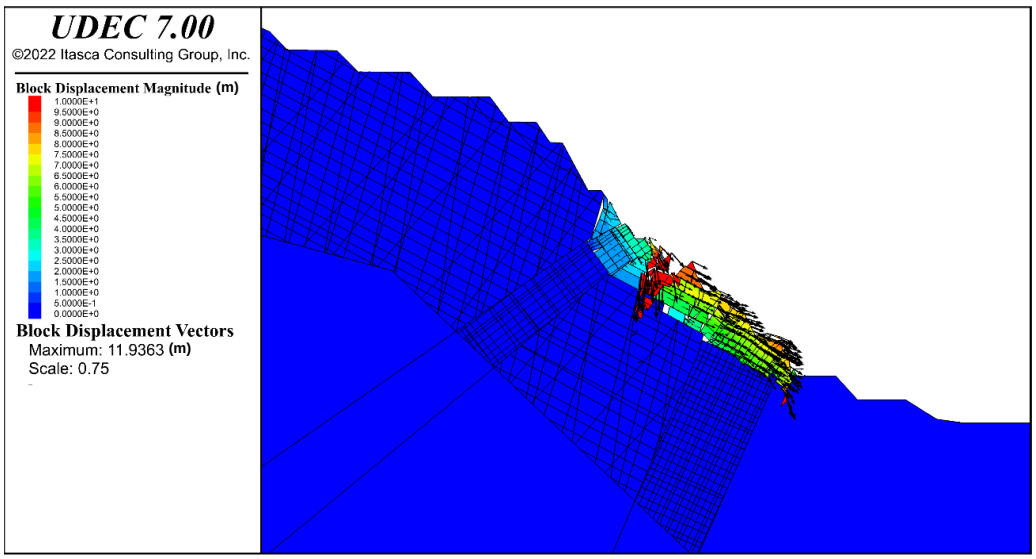

Figure 5. Model displacement contours and vectors.

The effectiveness of the stabilization measures (slope unloading between the 1221 and 1185 m benches, and buttress placement) was assessed in the post-stabilization simulations, assuming that the failure masses obtained from the back analyses would remain acting as driving forces on the buttress. All failed material discontinuities were modeled with $\Phi = 30°$, and σ_t and c of zero. This is extremely conservative as the slope conditions indicated little to no movement in the deformed state.

Model results indicate that the buttress would be able to stabilize the affected sector and that the layback would not impact stability in the upper slope. Figures 6 shows a maximum displacement within the buttress of up to 0.4 m. Additionally, the FOS for the post-stabilization analyses was calculated using the SSR method. According to the results, the static FOS is 1.17 as shown in Figure 6. This level of precision is provided to illustrate the model results.

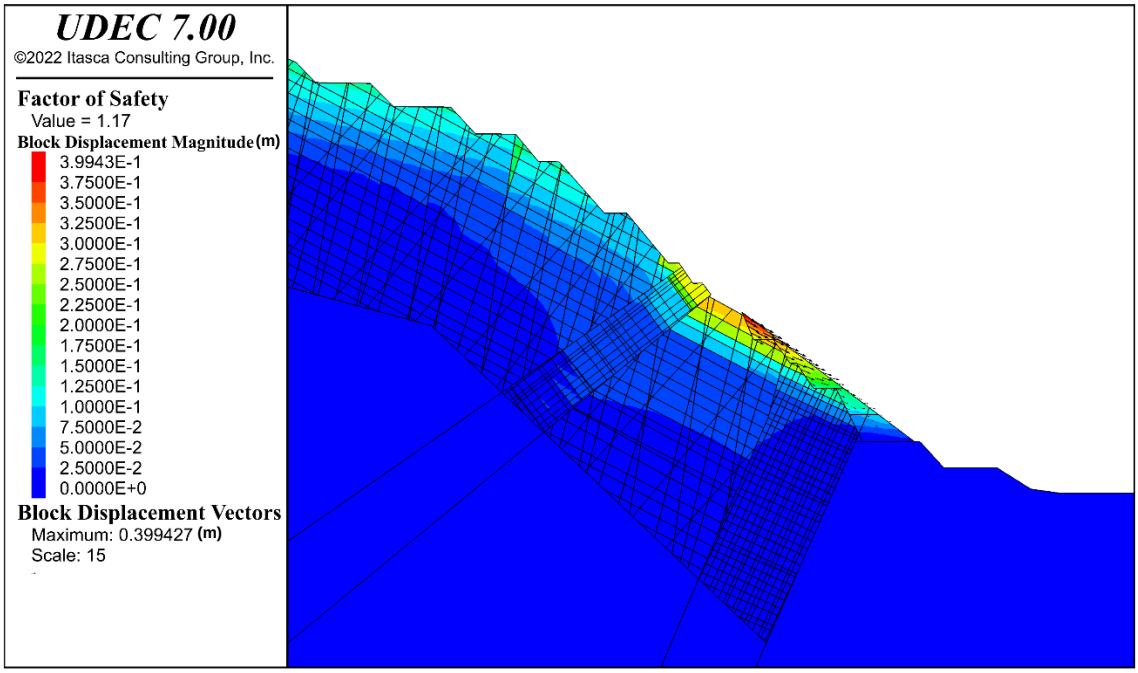

Figure 5. Buttress and layback model displacement contours, vectors, and FOS.

These are acceptable values for temporary support under static conditions. The pseudo-static analyses for the same cases returned FOS of 0.99 for the design peak ground acceleration. These factors of safety are considered acceptable given the short stand-up time for the buttress.

5 Conclusions

The models presented herein utilized the synthetic rock mass modeling approach to allow for realistic propagation of yield and failure without a specific user-prescribed failure plane. Following failure in FZ2, Lower Tuff, and FZ1, failure propagated to the same bench elevation as observed in the field and the upper slope displacements matched those measured by survey monuments above the failed bench. The lack of tedious calibration allowed for assessment of the efficacy of the proposed layback and buttress to allow the mine to advance safely to the pit to ultimate pit depth. A more in-depth study could consider varying the equivalent Mohr-Coulomb contact strength in the competent rock mass with depth, updating joint plane failure states based on adjacent block yield, and explicitly including perched groundwater to attempt to capture failure initiation as well as propagation.

6 References

ASTM D4767 - 11 Standard Test Method for Consolidated Undrained Triaxial Compression Test for Cohesive Soils.

ASTM D6323 - 19 Standard Guide for Laboratory Subsampling of Media Related to Waste Management Activities.

ASTM D6913 - 04 Standard Test Methods for Particle-Size Distribution (Gradation) of Soils Using Sieve Analysis.

Cremeens, J. (2003). *Geologic Controls on Complex Slope Displacement at the Pitch Reclamation Project. Engineering Geology in Colorado: Contributions, Trends, and Case Histories. AEG Journal. June 20, 2003*

Hoek E. et al. (2002). *Hoek-Brown Failure Criterion – 2002 Edition. Proc. NARMS-TAC Conference, Toronto, 2002, 1, 267-273.*

Hoek E. and Diederichs M.S. (2006). *Empirical Estimation of Rock Mass Modulus. International Journal of Rock Mechanics & Mining Sciences 43 (2006) 203–215.*

Itasca Consulting Group. (2019). *UDEC Version 7.00.79. UDEC 7.0 Documentation. file:///C:/Program%20Files/Itasca/UDEC700/exe64/doc/common/docproject/source/manual/program_guide/program_guide.html*

Kulhawy, F.H., 1975. *Stress Deformation Properties of Rock and Rock Discontinuities*. Eng. Geol., 9: 327-350.

Marinos, P. and Hoek, E. (2000). *GSI: A Geologically Friendly Tool for Rock Mass Strength Estimation. Proc. GeoEng2000 Conference, Melbourne.*